HHS Public Access

Author manuscript

Science. Author manuscript; available in PMC 2019 January 04.

Published in final edited form as:

Science. 2016 June 10; 352(6291): 1334–1337. doi:10.1126/science.aad9633.

Capture of A Third Mg^{2+} is Essential for Catalyzing DNA Synthesis

Yang Gao[1] and **Wei Yang**[1]

[1]Laboratory of Molecular Biology, NIDDK, National Institutes of Health, Bethesda, MD 20892

Abstract

It is generally assumed that an enzyme-substrate (ES) complex contains all components necessary for catalysis, and conversion to products occurs by rearrangement of atoms, protons and electrons. However, we find that DNA synthesis does not occur in a fully assembled DNA polymerase-DNA-dNTP complex with two canonical metal ions bound. Using time-resolved X-ray crystallography, we show that the phosphoryltransfer reaction takes place only after the ES complex captures a third divalent cation that is not coordinated by the enzyme. Interestingly, binding of the third cation is incompatible with the basal ES complex and requires thermal activation of the ES for entry. We suggest that the third cation provides the ultimate boost over the energy barrier to catalysis of DNA synthesis.

Enzymes increase the rate of chemical reaction, which is thought, to occur by reducing the activation energy required to reach the transition state (1–3) (Fig. 1A). Due to their transient and unstable nature, authentic transition states have not been visualized but are assumed to have the same chemical components as the substrate state. DNA polymerases, which catalyze a phosphoryltransfer reaction that incorporates dNTPs into DNA, are known to require two Mg^{2+} ions (4–8) (Fig. 1B). Despite extensive kinetic studies using the stopped flow technique and the dNTP analog dNTPαS, it remains controversial whether a conformational transition prior to catalysis (9–14) or the chemistry itself (15–16) is the rate-limiting step in DNA synthesis.

We have recently visualized phosphodiester bond formation catalyzed by human DNA Pol η *in crystallo* (17). Consistent with the two-metal-ion mechanism (6–8), binding of Mg^{2+} ions in the A and B sites occurs within 40 s leading to alignment of the 3′-OH of the primer end with the α-phosphate of dNTP (Fig. 1C) (17). After another 40 s, product starts to appear without discernible conformational change of the enzyme or substrates. However, we observed a third Mg^{2+} ion appearing in a third 'C' site after product formation (Fig. 1C) (17). An equivalent third metal ion coordinated by the reaction products and four water molecules has also been observed in the *in crystallo* catalysis by DNA Pol β (18–20). Due to steric clashes with dNTP (Fig. 1C), the third metal ion cannot bind in Pol η enzyme-substrate complexes. Because of low occupancy in the C site and weak diffraction of Mg^{2+} ions, it has been unclear when the third Mg^{2+} appears and whether it is involved in the phosphoryltransfer reaction.

Correspondence: wei.yang@nih.gov, Tel: (301) 402-4645, Fax: (301) 496-0201.

To determine the reaction coordinates of Pol η and the role of the third metal ion, we replaced Mg^{2+} with Mn^{2+}, which supports DNA synthesis (21) and is readily detected by X-ray diffraction even at low occupancy. Crystals of native Pol η (1–432 aa) complexed with DNA, dATP and Ca^{2+} were grown at pH 6.0 in a non-reactive ground state (17). After exposure to a pH 7.0 reaction buffer containing 1 mM Mn^{2+} for 90 to 1800 s, crystals were flash frozen in liquid N_2 to stop the reaction, and 1.5–1.7 Å X-ray structures were determined at five reaction time points (table S1 and Materials and Methods). All five structures were practically identical except for the gradual replacement of Ca^{2+} by Mn^{2+} in the B site (fig. S1). By 600 s when ~90% of the A and B sites were occupied by Mn^{2+}, the 3´-OH of the DNA primer was aligned with the α-phosphorus of the dATP, and the structure was identical to that of crystals soaked in 1 mM Mg^{2+} for 40 s (fig. S2, A-B). Similar to the reaction in Mg^{2+} (17), a water molecule (WatN) hydrogen bonded to the nucleophilic 3´-OH appeared at 90 s, and its occupancy increased with time in correlation with binding of the A-site Mn^{2+} (fig. S2, C-D). However, in 1 mM Mn^{2+}, the Pol η-DNA complex remained in the substrate state with no product and no C-site Mn^{2+} ion for up to 1800s (Fig. 1D).

We assayed the metal ion (Me^{2+}) requirements for Pol η catalysis in solution and found that 0.6 mM Mg^{2+} or 2.7 mM Mn^{2+} is needed to attain the half-maximal reaction rate (Fig. 2A, table S2). We then examined the Mn^{2+} affinity of each binding site *in crystallo*. While increasing the Mn^{2+} concentration (0.5 to 15 mM) accelerated the rate of metal-ion binding in all three sites (Fig. 2B, table S3), the apparent K_d's of the A and B sites were below 0.5 mM. The K_d for the C site, however, was 3.2 mM, close to the 2.7 mM measured in solution (Fig. 2A).

When *in crystallo* reactions occurred in 10 mM Mn^{2+}, catalysis proceeded as in 1 mM Mg^{2+} (17), except that the A-site Mn^{2+} did not dissociate upon product formation as does Mg^{2+} (fig. S3, A-B) and slightly less product accumulated with Mn^{2+} than Mg^{2+}. However, unlike the reaction in Mg^{2+}, the C-site Mn^{2+} appeared simultaneously with the reaction product, 30 s after binding of the two canonical metal ions (Fig. 2C). Electron density for the new phosphodiester bond and the C-site Mn^{2+}, whose chemical nature was confirmed by its anomalous diffraction and characteristic octahedral coordination geometry (fig. S3C), had one-to-one correlation at every time point and Mn^{2+} concentration (Fig. 2D). In Mg^{2+} by contrast, with 15% product formed at 80 s the C-site Mg^{2+} was at too low occupancy to be observed and was not detected until 140 s when product had accumulated to 40% (fig. S3A) (17). Previous stopped-flow studies indicate that one of the metal ion-binding sites has much lower affinity for Mg^{2+} and thus limits DNA synthesis (16). Our *in crystallo* titrations unequivocally show that the low-affinity binding site is neither A nor B, but the C site, which determines the concentration of Mg^{2+} or Mn^{2+} necessary for the DNA synthesis reaction.

The C-site Me^{2+} is coordinated by four water molecules and two oxygen atoms, one each from the product DNA and pyrophosphate, which correspond to the α pro-S_p oxygen and the α, β bridging oxygen of dNTP (Fig. 1C). Sulfur substitution of the pro-S_p oxygen (S_p-dNTPαS) has been widely used to dissect the reaction kinetics of DNA synthesis (11–14, 22) because the pro-S_p atom is not directly involved in A- or B-site Me^{2+} coordination. The

reduction of the reaction rate by S_p-dNTPαS has been interpreted to be "conformational" (if < 4 fold reduction) or to affect the chemistry itself (if 4–11 fold) (11–14, 23).

As a ligand of the 3rd Me^{2+}, the sulfur in S_p-dATPαS was tolerated by Pol η (table S2) but required much higher [Mg^{2+}] (15 mM) and [Mn^{2+}] (9 mM) than dATP for catalysis to occur (Fig. 2A, Fig. 3A). Unexpectedly, *in crystallo* S_p-dATPαS slowed Mg^{2+} and Mn^{2+} binding at the A site. After a lengthened delay product started to form, but the C site remained empty (Fig. 3B, fig. S4A-C). We suspect that the third Mn^{2+} still assisted product formation, but the association was too transient to be observed. In addition, while A-site Mg^{2+} occupancy was reduced in the presence of dATPαS, an alternative A' site appeared 2.6 Å away (fig. S4, D-E). These data suggest that the reduced reaction rate with S_p-dATPαS cannot be attributed to "conformational" effects (11–14) but involves impaired A- and C-site Mg^{2+} binding and altered reaction chemistry.

To bind the third Me^{2+}, the R61 side chain, which forms salt bridges with the dNTP (17), moves to vacate the C site (Fig. 1C, 3B). Mutation of R61 to Ala reduces the k_{cat} by two thirds (table S2) (24–25), but the metal-ion requirement and the general reaction process *in crystallo* were indistinguishable from WT Pol η (fig. S5E-F). However, the delay between binding of two Mg^{2+} ions and product formation was lengthened from WT's 40 s to R61A's 160 s (Fig. 3C). This delay likely stems from a slight shift of dATP away from the active site and a 0.3 Å increase in separation between the 3′-OH and α-phosphate (Fig. 3D). The void left by the R61A mutation was occupied by water molecules (25) and not by the abundant K^+ or Rb^+ (identifiable by anomalous diffraction) in the reaction buffer (fig. S5). The subtle misalignment of the substrate, which was repeatedly observed with R61A and R61M mutant Pol η (25) and with dATPαS, led to a prolonged delay before C-site Me^{2+} binding and product formation (fig. S4, B-C).

Notably a +1 charged side chain at the position equivalent to R61 is found in all A-, B-, and Y-family DNA polymerases and reverse transcriptases despite diverse structures of finger domains surrounding the C-site (fig. S6). Among C- and X-family DNA polymerases, there is no R61 equivalent, but the third metal ion has been observed for the X-family Pol β (18–20). The finger domains, which carry the +1 charged residue, distinguish right from wrong correct from incorrect incoming nucleotides by enclosing only a correct dNTP (26). A closed finger appears to be a prerequisite for C-site metal ion binding and catalysis. The varied environment surrounding the C site may thus be exploited for drug design to increase specificity and reduce toxicity of broadly used nucleoside and nucleotide analogs targeting DNA polymerases in antiviral and anti-cancer therapeutics (27–28).

Because the C site does not exist in the Pol η-substrate complex but is required for product formation, we hypothesized that thermal motion of the well-aligned reactants in the ES may create an opening for the 3rd metal ion. If so, elevated temperature would promote C-site metal ion binding and thus catalysis. To test this hypothesis, we designed a two-step *in crystallo* reaction. The Pol η crystals were first soaked in 1 mM Mn^{2+} to saturate the A and B sites, and then exposed to 5 mM Mn^{2+} at 4°C to 37°C for 60 s for catalysis to occur (Fig. 4A). The diffusion rate of Mn^{2+} *in crystallo* was unaffected by temperature as demonstrated by Mn^{2+} binding at the A-site (Fig. 4B). But in the two-step reaction, no C-site Mn^{2+} or

product was detected at 4°C (Fig. 4C). At 14°C, low levels of the third Mn^{2+} ion and products were observed, and their amounts doubled at 30°C. The temperature dependence of C-site and product formation corroborates that binding of the third metal ion is rate limiting in the DNA synthesis reaction.

To determine the metal ion selectivity at the C site, we varied Me^{2+} in the second step of the two-step reaction (Fig. 4A). Catalysis occurred most efficiently with Mg^{2+}, followed by Mn^{2+} and Cd^{2+} (Fig. 4D, fig. S7). Ca^{2+} and Zn^{2+} seemingly also led to product formation at ~40% efficiency of Mg^{2+}. However, the C-site coordination geometry with all five Me^{2+} tested appeared identical to that of Mg^{2+} and Mn^{2+} (fig. S7) despite different coordination distances of Ca^{2+} (2.3–2.5Å) and Mg^{2+} or Mn^{2+} (2.1Å). It is thus likely that Ca^{2+} and Zn^{2+} replaced A or B site Mn^{2+} in some Pol η molecules, and the freed Mn^{2+} ions may occupy the C site in other Pol η molecules to support the catalysis. The low affinity and strong preference for Mg^{2+} at the C site, which cannot be explained by its coordination ligands, suggest a catalytic role for the third metal ion in DNA synthesis.

Based on the requirement for three metal ions in DNA synthesis, we suggest a revision of the catalytic mechanism (Fig. 5). DNA synthesis begins with binding of dNTP along with the B-site Mg^{2+} and formation of a ground-state Pol η-DNA-dNTP-Mg^{2+} complex (GS). Watson-Crick pairing between the template and dNTP favors A-site Mg^{2+} binding. The two Mg^{2+} ions and the R61 side chain neutralize and align dNTP with DNA in the reaction-ready state (ES), where the juxtaposed and polarized substrates recruit WatN (fig. S2) (17). However, neither deprotonation nor chemistry takes place without the C-site Mg^{2+}. Thermal motion may transiently bring the perfectly aligned reactants closer to each other by fractions of an Ångstrom and create an entry for the third Mg^{2+}. Close approach of the reactants may also increase negative charge around the α-phosphate and favor replacement of the +1 charged R61 by the C-site Mg^{2+}. We hypothesize that the energy barrier to the transition state is overcome by binding of the third Mg^{2+}. The stringent octahedral coordination geometry of Mg^{2+} implies that the C-site Mg^{2+} may help to break the α-β phosphodiester bond (Fig. 5) in addition to protonating the pyrophosphate leaving group (17). Product formation is coupled to disappearance of WatN (fig. S3D), which likely deprotonates the 3´-OH, and to release of the A-site Mg^{2+}, which prevents the reverse reaction (fig. S3, A-B).

It has long been assumed that enzymes stabilize transition states and reduce the energy barrier to product formation (Fig. 1A), but de novo design of enzymes based on this assumption has not been successful (29–32). Notwithstanding its crucial role in catalysis, the C-site metal ion of polymerases has evaded detection by biochemical and structural studies of DNA polymerases for decades. Identification of the essential third metal ion in the Pol η catalysis leads us to anticipate that acquisition of transient metal-ion cofactors in transition states may be a general feature that enables enzyme catalysis.

Supplementary Material

Refer to Web version on PubMed Central for supplementary material.

Acknowledgements

Y.G. carried out all experiments; W.Y. conceived and designed the project, and both authors interpreted data and prepared the manuscript. We thank D. J. Leahy and M. Gellert for critical reading and editing the manuscript. This work is funded by NIH intramural program (DK036146–08, W.Y.).

Reference

1. Garcia-Viloca M, Gao J, Karplus M, Truhlar DG, How enzymes work: analysis by modern rate theory and computer simulations. Science 303, 186–195 (2002)
2. Benkovic SJ, Hammes-Schiffer S, A Perspective on Enzyme Catalysis. Science 301, 1196–1202 (2003) [PubMed: 12947189]
3. Warshel A et al., Electrostatic basis for enzyme catalysis. Chem. Rev 106, 3210–3235 (2006). [PubMed: 16895325]
4. Rothwell PJ, Waksman G, Structure and mechanism of DNA polymerases. Adv. Protein Chem 71, 401–440 (2005). [PubMed: 16230118]
5. Tsai MD, How DNA polymerases catalyze DNA replication, repair, and mutation. Biochemistry 53, 2749–2751 (2014) [PubMed: 24716436]
6. Steitz TA, Steitz JA, A general two-metal-ion mechanism for catalytic RNA. Proc. Natl Acad. Sci. USA 90, 6498–6502 (1993). [PubMed: 8341661]
7. Steitz TA, DNA polymerases: structural diversity and common mechanisms. J. Biol. Chem 274, 17395–17398 (1999). [PubMed: 10364165]
8. Yang W, Lee JY, Nowotny M, Making and breaking nucleic acids: two-Mg^{2+}-ion catalysis and substrate specificity. Mol. Cell 22, 5–13 (2005)
9. Joyce CM, Benkovic SJ, DNA polymerase fidelity: kinetics, structure, and checkpoints. Biochemistry 43, 14317–14324 (2004). [PubMed: 15533035]
10. Johnson KA, Role of induced fit in enzyme specificity: a molecular forward/reverse switch. J. Biol. Chem. 283, 26297–26301 (2008). [PubMed: 18544537]
11. Patel SS, Wong I, Johnson KA, Pre-steady-state kinetic analysis of processive DNA replication including complete characterization of an exonuclease-deficient mutant. Biochemistry 30, 511–525 (1991). [PubMed: 1846298]
12. Dahlberg ME, Benkovic SJ, Kinetic mechanism of DNA polymerase I (Klenow fragment): identification of a second conformational change and evaluation of the internal equilibrium constant. Biochemistry 30, 4835–4843 (1991). [PubMed: 1645180]
13. Washington MT, Prakash L, Prakash S, Yeast DNA polymerase η utilizes an induced-fit mechanism of nucleotide incorporation. Cell 107, 917–927 (2001). [PubMed: 11779467]
14. Fiala KA, Suo Z, Mechanism of DNA polymerization catalyzed by *Sulfolobus solfataricus* P2 DNA polymerase IV. Biochemistry 43, 2116–2125 (2004) [PubMed: 14967051]
15. Rothwell PJ, Mitaksov V, Waksman G. Motions of the fingers subdomain of klentaq1 are fast and not rate limiting: implications for the molecular basis of fidelity in DNA polymerases. Mol. Cell 19, 345–355 (2005). [PubMed: 16061181]
16. Bakhtina M et al., Use of viscogens, dNTPalphaS, and rhodium(III) as probes in stopped-flow experiments to obtain new evidence for the mechanism of catalysis by DNA polymerase beta. Biochemistry 44, 5177–5187 (2005). [PubMed: 15794655]
17. Nakamura T, Zhao Y, Yamagata Y, Hua YJ, Yang W, Watching DNA polymerase η make a phosphodiester bond. Nature 487, 196–201 (2012). [PubMed: 22785315]
18. Freudenthal BD, Beard WA, Shock DD, Wilson SH, Observing a DNA polymerase choose right from wrong. Cell 154, 157–168, (2013). [PubMed: 23827680]
19. Freudenthal BD et al., Uncovering the polymerase-induced cytotoxicity of an oxidized nucleotide. Nature 517, 635–639 (2015). [PubMed: 25409153]
20. Vyas R, Reed AJ, Tokarsky EJ, Suo Z, Viewing human DNA polymerase β faithfully and unfaithfully bypass an oxidative lesion by time-dependent crystallography. J. Am. Chem. Soc. 137, 5225–5230 (2015). [PubMed: 25825995]

21. Cowan JA, Metal activation of enzymes in nucleic acid biochemistry. Chem. Rev 98, 1067–1087 (1998). [PubMed: 11848925]
22. Burgers PM, Eckstein F, Absolute configuration of the diastereomers of adenosine 5'-O-(1-thiotriphosphate): consequences for the stereochemistry of polymerization by DNA-dependent RNA polymerase from Escherichia coli. Proc Natl Acad Sci U S A. 75, 4798–4800, (1978). [PubMed: 368798]
23. Herschlag D, Piccirilli JA, Cech TR, Ribozyme-catalyzed and nonenzymatic reactions of phosphate diesters: rate effects upon substitution of sulfur for a nonbridging phosphoryl oxygen atom. Biochemistry 30, 4844–4854 (1991). [PubMed: 2036355]
24. Biertumpfel C et al., Structure and mechanism of human DNA polymerase η. Nature 465, 1044–1048 (2010). [PubMed: 20577208]
25. Su Y, Patra A, Harp JM, Egli M, Guengerich FP, Roles of residues Arg-61 and Gln-38 of human DNA polymerase η in bypass of deoxyguanosine and 7,8-dihydro-8-oxo-2'-deoxyguanosine. J. Biol. Chem 290, 15921–15933 (2015) [PubMed: 25947374]
26. Wu EY, Beese LS, The structure of a high fidelity DNA polymerase bound to a mismatched nucleotide reveals an "ajar" intermediate conformation in the nucleotide selection mechanism. J. Biol. Chem 286, 19758–19767 (2011) [PubMed: 21454515]
27. Kakuda TN, Pharmacology of nucleoside and nucleotide reverse transcriptase inhibitor-induced mitochondrial toxicity. Clin. Ther 22, 685–708 (2000) [PubMed: 10929917]
28. Jordheim LP, Durantel D, Zoulim F, Dumontet C, Advances in the development of nucleoside and nucleotide analogues for cancer and viral diseases. Nat. Rev. Drug Discov 12, 447–464 (2013) [PubMed: 23722347]
29. Wagner J, Lerner RA, Barbas CF, 3rd, Efficient aldolase catalytic antibodies that use the enamine mechanism of natural enzymes. Science 270, 1797–1800 (1995) [PubMed: 8525368]
30. Bolon DN, Mayo SL, Enzyme-like proteins by computational design. Proc. Natl. Acad. Sci. U.S.A 98, 14274–14279 (2001) [PubMed: 11724958]
31. Jiang L et al., *De novo* computational design of retro-aldol enzymes. Science 319, 1387–1391 (2008) [PubMed: 18323453]
32. Rothlisberger D et al., Kemp elimination catalysts by computational enzyme design. Nature 453, 190–195 (2008) [PubMed: 18354394]
33. Kabsch W, XDS. Acta Crystallogr. D 66, 125–132 (2010) [PubMed: 20124692]
34. Adams PD et al., PHENIX: a comprehensive Python-based system for macromolecular structure solution. Acta Crystallogr. D 66, 213–221 (2010) [PubMed: 20124702]
35. Emsley P, Lohkamp B, Scott WG, Cowtan K, Features and development of Coot. Acta Crystallogr. D 66, 486–501 (2010) [PubMed: 20383002]
36. Howell L, & Smith D, Normal probability analysis. J. Appl. Cryst 25, 81–86 (1992)
37. Collaborative Computational Project Number 4. The CCP4 suite: programs for protein crystallography. Acta Crystallogr. D 50, 760–763 (1994). [PubMed: 15299374]
38. Li Y, Korolev S, Waksman G, Crystal structures of open and closed forms of binary and ternary complexes of the large fragment of Thermus aquaticus DNA polymerase I: structural basis for nucleotide incorporation. EMBO J. 17, 7514–7525 (1998) [PubMed: 9857206]
39. Wang F, Yang W, Structural insight into translesion synthesis by DNA Pol II. Cell 139, 1279–1289 (2009) [PubMed: 20064374]
40. Huang H, Chopra R, Verdine GL, Harrison SC, Structure of a covalently trapped catalytic complex of HIV-1 reverse transcriptase: implications for drug resistance. Science 282, 1669–1675 (1998) [PubMed: 9831551]
41. Lansdon EB et al.,Structural and Binding Analysis of Pyrimidinol Carboxylic Acid and N-Hydroxy Quinazolinedione HIV-1 RNase H Inhibitors. Antimicrob. Agents Chemother. 55, 2905–2915 (2011) [PubMed: 21464257]
42. Beard WA, Shock DD, Batra VK, Pedersen LC, Wilson SH, DNA polymerase beta substrate specificity: side chain modulation of the "A-rule". J. Biol. Chem 284, 31680–31689 (2009) [PubMed: 19759017]

43. Evans RJ et al., Structure of PolC reveals unique DNA binding and fidelity determinants. Proc. Natl. Acad. Sci. USA 105, 20695–20700 (2008) [PubMed: 19106298]

44. Bailey S, Wing RA, Steitz TA, The structure of T aquaticus DNA polymerase III is distinct from eukaryotic replicative DNA polymerases. Cell 126, 893–904 (2006) [PubMed: 16959569]

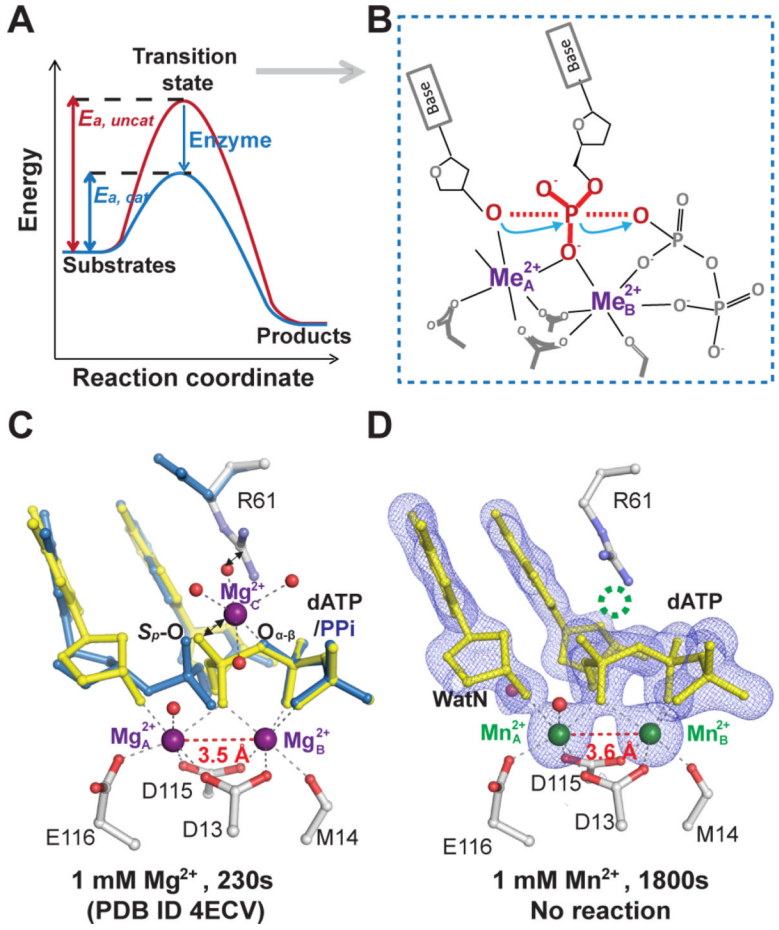

Figure 1 |. No DNA synthesis without the third metal ion.

A, Reaction coordinate of enzyme catalysis. **B**, The assumed transition state of the two-metal-ion catalysis. **C**, The structure of Pol η catalyzing DNA synthesis *in crystallo* (PDB: 4ECV, 18). The C-site Mg^{2+} is coordinated by the products (60%, blue) but clashes with the substrate dATP and R61 side chain (40%, yellow). **D**, The structure of Pol η incubated with substrates and 1 mM Mn^{2+} for 1800s. No C-site metal ion or reaction products were detected. The F_O-F_C map with the active center omitted contoured at 3.5σ level (blue meshes) is superimposed.

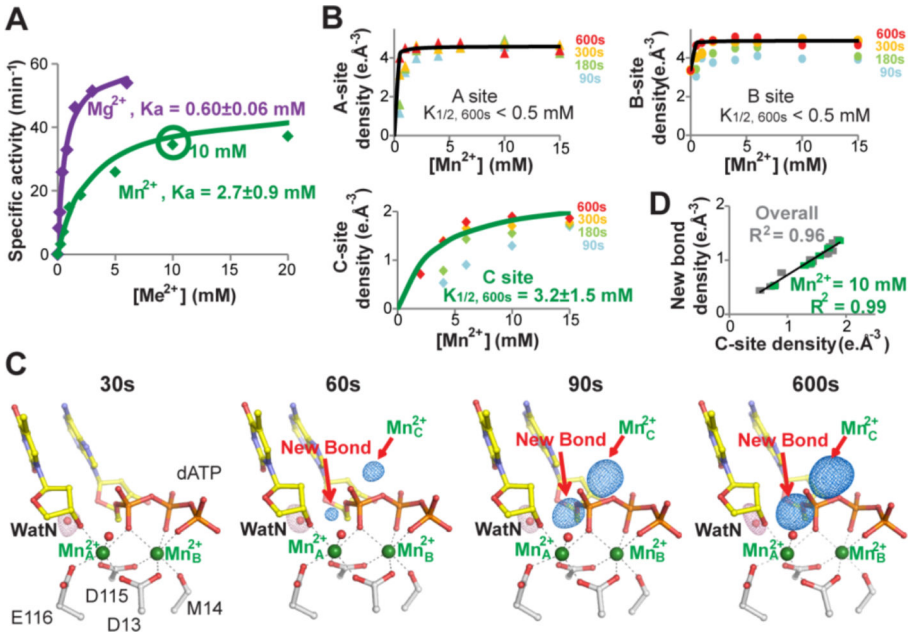

Figure 2 |. Coupled appearance of the third Mn^{2+} and reaction products.

A, Mg^{2+} (purple) and Mn^{2+} (green) dependence of Pol η catalysis in solution. **B**, Titration of the A-, B-, and C-site Mn^{2+} binding *in crystallo*. The 600s data were fitted to equilibrium binding modes to yield the K_d's. **C**, Structures of Pol η *in crystallo* catalysis with 10 mM Mn^{2+}. The F_o-F_c omit map for the new bond, the C-site Mn^{2+} (blue) and the WatN (pink) were contoured at 3σ and superimposed onto each structure. **D**, Correlation between the new bond formation and the C-site Mn^{2+} binding.

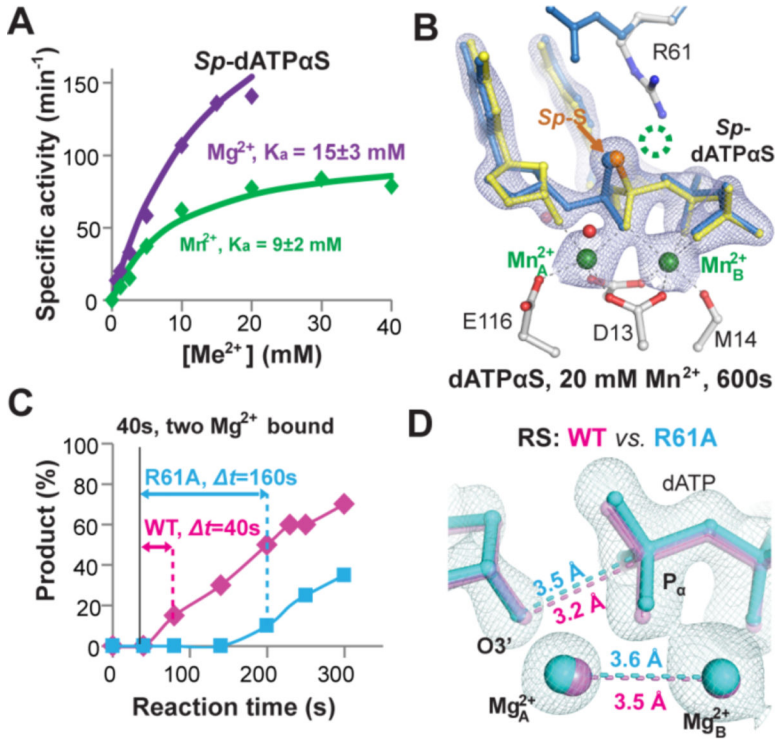

Figure 3 |. Changing the C-site environment alters Pol η catalysis.

A, Mg^{2+} (purple) and Mn^{2+} (green) dependence of Pol η incorporating dATPαS in solution. **B**, *In crytallo* incorporation of dATPαS by Pol η with 20 mM Mn^{2+} at 600s showed product formation (50%) but no C-site Mn^{2+}. The $2F_o$-F_c map contoured at 2σ level (blue meshes) is superimposed. **C**, Time delay in product formation by WT (magenta) and R61A (cyan) Pol η *in crystallo*. **D**, Deviation of dATP in the ES of R61A Pol η (cyan with $2F_o$-F_c map contoured at 1.5σ) from WT Pol η (magenta).

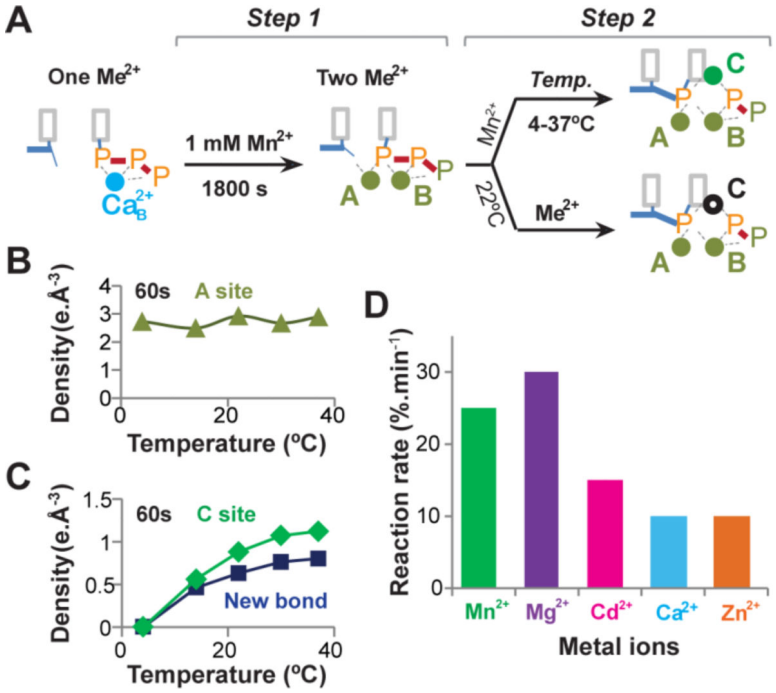

Figure 4 |. Thermal energy-dependent C-site formation and its metal-ion selectivity.

A, Schematic diagram of the two-step *in crystallo* reactions that probe the C-site formation and ion selectivity. **B**, Binding of the A-site Mn^{2+} was unaffected by varying temperature from 4°C to 37°C. **C**, Binding of the C-site Mn^{2+} and the product formation increased with the temperature from 4°C to 37°C. **D**, Rates of product formation with five metal ions tested in the second step.

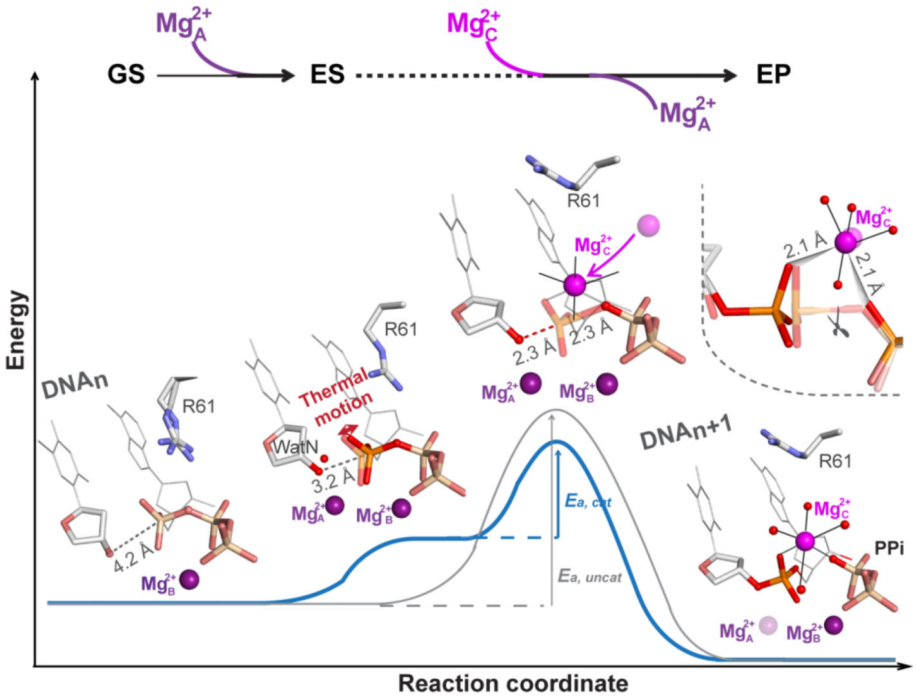

Figure 5 |. Mechanism of Pol η catalysis.

Pol η binds DNA and an incoming dNTP along with the B-site Mg^{2+} to form the ground state (GS). Binding of the A-site Mg^{2+} leads to the reaction-ready ES state, in which the 3'-OH is aligned with dNTP and WatN recruited. Thermal motions of the reactants create the C site, leading to the third metal-ion binding and the transition state (TS) formation. The C-site metal ion promotes the phosphoryltransfer from the leaving group to the nucleophilic 3´-OH, thus overcoming the energy barrier to the product state (PS).